

**Suppression of Shuttle Effect in Li-S Battery: A Combined
Machine-Learning and DFT Approach for High Throughput
Screening of Cathode Host Materials**

M.Sc. Thesis

By
ADARSH SONKAR



**DEPARTMENT OF CHEMISTRY
INDIAN INSTITUTE OF TECHNOLOGY INDORE**

MAY 2023

Suppression of Shuttle Effect in Li-S Battery: A Combined Machine-Learning and DFT Approach for High Throughput Screening of Cathode Host Materials

A THESIS

Submitted in partial fulfillment of the requirements for the award of the degree
of
MASTER OF SCIENCE

by
ADARSH SONKAR



DEPARTMENT OF CHEMISTRY
INDIAN INSTITUTE OF TECHNOLOGY INDORE

MAY 2023



INDIAN INSTITUTE OF TECHNOLOGY INDORE

CANDIDATE'S DECLARATION

I hereby certify that the work which is being presented in the thesis entitled **Suppression of Shuttle Effect in Li-S Battery: A Combined Machine-Learning and DFT Approach for High throughput screening of Cathode Host Materials** in the partial fulfillment of the requirements for the award of the degree of **MASTER OF SCIENCE** and submitted in the **DEPARTMENT OF CHEMISTRY, Indian Institute of Technology Indore**, is an authentic record of my own work carried out during the time period from **July 2022 to May 2023** under the supervision of Prof. Dr. Biswarup Pathak, Professor, Department of Chemistry, Indian Institute of Technology Indore.

The matter presented in this thesis has not been submitted by me for the award of any other degree of this or any other institute.


Signature of the student with date
(Adarsh Sonkar)

This is to certify that the above statement made by the candidate is correct to the best of my knowledge.


Signature of the Supervisor of M.Sc. thesis with date
(Prof. Dr. Biswarup Pathak)

Adarsh Sonkar has successfully given his M.Sc. Oral Examination held on

17th May 2023.


Signature of Supervisor of M.Sc. thesis
Prof. Biswarup Pathak
Date:


Signature of PSPC Member
Prof. Sanjay Kumar Singh
Date:


Convener, DPGC
Dr. Umesh A. Kshirsagar
Date: 30/05/2023


Signature of PSPC Member
Dr. Tridib Kumar Sarma
Date:

Acknowledgments

With immense delight, I express my utmost appreciation to my esteemed thesis supervisor, Professor Biswarup Pathak, who is a renowned expert in the field of chemistry and currently serves as a professor at the Indian Institute of Technology Indore. His exceptional guidance, timely support, and unbridled motivation have been invaluable in my successful completion of this M.Sc. project. His profound enthusiasm and unwavering dedication have always been a source of inspiration for me.

I would also like to extend my heartfelt thanks to the members of my thesis committee, Professor Sanjay Kumar Singh, and Dr. Tridib Kumar Sarma, for their invaluable suggestions and unwavering support throughout my research project.

I am immensely grateful to the current Director of Indian Institute of Technology Indore, Professor Suhas S. Joshi for their encouragement and provision of the necessary facilities and resources for my research work.

I would like to acknowledge the Indian Institute of Technology Indore for providing the state-of-the-art laboratory and computational facilities that were crucial in facilitating my research project.

My sincere gratitude also goes to the Head of the Department of Chemistry, Indian Institute of Technology Indore, for their constant motivation and creation of a conducive research environment. I would also like to extend my thanks to Professor Rajneesh Misra, Professor Suman Mukhopadhyay, Professor Apurba K. Das, Professor Sampak Samanta, Dr. Anjan Chakraborty, Dr. Tushar Kanti Mukherjee, Dr. Shaikh M. Mobin, Dr. Satya S. Bulusu, Dr. Chelvam Venkatesh, Dr. Amrendra Kumar Singh, Dr. Abhinav Raghuvanshi, Dr. Dipak Kumar Roy, Dr. Selvakumar Sermadurai, Dr. Umesh A. Kshirsagar, Dr. Debayan Sarkar, Dr. Pravarthana Dhanpal, and Dr Soumen Ghosh for their expert guidance and unwavering support throughout my M.Sc. course. The professional

support of the Chemistry office staffs, Mr. Manish Kushwaha, Mr. Parthiban P. K., Ms. Vinita Kothari, Priyanka Tayde and Mr. Rameshwar Dauhare, were also highly appreciated.

I owe a special debt of gratitude to my project mentor, Mr. Souvik Manna and Mr. Sandeep Das for his exceptional guidance and support throughout the project. With boundless gratitude, I express my sincere appreciation to the following senior lab members: Dr. Mohan Tiwari, Mr. Arunendu Das, Mr. Surya Shekhar Manna, Mr. Amitabha Dass, Mr. Milan Kumar Jena, Mrs. Nishchal Bharadwaj, Ms. Eti Mahal, Ms. Sneha Mittal, Ms. Harpriya Minhas, and Mr. Rahul Kumar Sharma, for their exceptional contributions, support, and guidance in every aspect of my project. Their invaluable insights and expertise have undoubtedly enriched my research journey, and their camaraderie, encouragement, and astounding support have been instrumental in driving me to strive for excellence.

I would like to express my admiration to all my batchmates, juniors, and PhDs who shared this journey with me, as they provided excellent academic and social support throughout my M.Sc. program.

Finally, my heartfelt appreciation goes to my family, including my parents, Mr. Vats Raj Sonkar, and Swaran Lata Sonkar, my two elder brothers Mr. Akash and Mr. Nitin, and my special friends Piku, Garv, Adshi, and Anishka for their unwavering support, trust, and encouragement throughout my academic journey.

ADARSH SONKAR



Dedicated
To
My Parents and CMDG Group



Abstract

The shuttle effect is a major issue in Lithium Sulfur battery that impedes practical implementation due to rapid capacity loss. The discovery of novel cathode host materials through complex experimental techniques is inefficient to find suitable cathode anchoring materials. Here, we propose a combined approach of machine learning (ML) and density functional theory (DFT) to discover appropriate sulfur host cathode materials that can effectively suppress the shuttle effect in Li-S batteries. This method aims to improve the search for suitable materials and enhance the efficiency of the discovery process. We applied a classification model to investigate the adsorption of polysulfides (Li_2S , Li_2S_2 , Li_2S_4 , Li_2S_6 , Li_2S_8 , S_8) on various layered double hydroxide (LDH) materials. We have found that Gradient Boosting model is suitable for predicting cathode host materials with optimum adsorption energy, while the perfectly fitted Adaboost model predicts stable cathode host materials. By combining two classification models 22 materials have been screened out through ML having high potential to be suitable sulfur host cathode materials. Finally, we cross-validated with DFT and proposed 16 cathode host materials out of 74 LDH materials are highly viable for the suppression of the shuttle effect. The combined ML-DFT method delivers high-precision and quick solutions for high-throughput screening based on adsorption energy.

Table of Contents

A. List of Figures	ix
B. List of Tables	xi
D. Acronyms	xiii
1. CHAPTER 1: Introduction	1
1.1. Lithium Sulfur Battery	3
1.2. Layered Double Hydroxide (LDH)	4
1.3. Artificial Intelligence (AI)	5
1.3.1. Machine Learning (ML)	6
1.3.1.1. Supervised Learning	7
1.3.1.1.1. Classification	7
1.3.1.2. ML Models	8
1.3.1.3. Testing and Validation	16
1.3.1.4. Hyperparameter Tuning	16
2. CHAPTER 2: Computational Methods and Approximations	17
2.1. Many-body Schrodinger Equation	17
2.2. Born-Oppenheimer Approximation	19
2.3. Hartree-Fock (HF) Approximation	19
2.4. Density Functional Theory (DFT)	20
2.4.1. The Hohenberg-Kohn Theorems	21
2.4.2. Kohn-Sham Formulation	22
2.4.3. Local Density Approximation (LDA)	22
2.4.4. Generalized Gradient Approximation (GGA)	23
2.5. Basis Sets	23
2.5.1. Projector Augmented Wave (PAW) Method	24
2.6. GPAW and ASE	25

2.7. DFT Details	25
3. CHAPTER 3: Results and Discussion	27
3.1. Materials selection	27
3.2. Features Engineering ML Model Selection	30
3.3. Host material prediction via ML classification	31
4. CHAPTER 4: Conclusions	41
5. APPENDIX– A	43
6. REFERENCES	47

List of Figures

CHAPTER 1

- Figure 1.1** The flowchart of the work. 3
- Figure 1.2** The depiction of the domain comprising DL, ML, and AI. 6
- Figure 1.3** A schematic diagram of a Multi-Layer Perceptron (MLP). 9
- Figure 1.4** A visual representation of a perceptron. 10
- Figure 1.5** The working mechanism of an Adaboost classifier is depicted in a flowchart format. 15

CHAPTER 2

CHAPTER 3

- Figure 3.1** Illustrating the top and side views of two distinct types of LDH material. 28
- Figure 3.2** Adsorption configuration of lithium-polysulfides on $[\text{Mg}_{20}\text{Al}_4(\text{OH})_{48}]$ -LDH host material. 29
- Figure 3.3** Pearson correlation coefficient (PCC) heat map of the considered features for this work. 31
- Figure 3.4** (a) Confusion matrix of test dataset and (b) feature importance scores of the considered features for class-A classification. 34
- Figure 3.5** (a) Confusion matrix of test dataset and (b) feature importance scores of the considered features for class-B classification. 36

CHAPTER 4

APPENDIX – A

Figure A1 Pearson correlation coefficient (PCC) heat map plot 43
considered before features engineering.

Figure A2 Optimized structures of Li_2S_6 adsorbed on 16 44
substrates.

List of Tables

CHAPTER 1

CHAPTER 2

CHAPTER 3

- Table 3.1** Accuracy score of distinct models based on 4 different train and test split (Set-1, Set-2, Set-3, and Set-4). 32-33
- Table 3.2** Accuracy score of various ML models for the classification of stable and unstable LDH materials on four distinct train and test splits. 35
- Table 3.3** Mean accuracy for each fold of 10-fold cross-validation using GB-classifier for class-A classification and AB-classifier for class-B classification. 37
- Table 3.4** Predicted outcome by ML model with probability of getting 1 for each class and cross verified by DFT predicted AE. 39

CHAPTER 4

APPENDIX – A

- Table A1** List of features that were used for the ML model. Abbreviations used in the manuscript to represent the features are given in parentheses. 44-45
- Table A2** Hyperparameter used in tuning the Gradient Boosting model. 46
- Table A3** Hyperparameter used in tuning the AdaBoost model. 46

Acronyms

ABC	AdaBoost Classifier
AE	Adsorption Energy
AI	Artificial Intelligence
ASE	Atomic Simulation Environment
DFT	Density Functional Theory
GBC	Gradient Boosting Classifier
GGA	Generalized Gradient Approximation
GPAW	Grid-Based Projector Augmented Wave
KNN	K-Nearest Neighbors
LDH	Layered Double Hydroxide
LDA	Linear Discriminant Analysis
Li-S	Lithium Sulfur
ML	Machine Learning
PCC	Pearson correlation coefficient
PBE	Perdew-Burke-Ernzerhof
PAW	Projector Augmented Wave
RFC	Random Forest Classifier
SGD	Stochastic Gradient Descent
SVC	Support Vector Classifier
VASP	Vienna ab-initio simulation package
XG Boost	Xtreme Gradient Boosting

1. Introduction

The expansion of the worldwide economy has stimulated a surge in industrialization and commercialization, necessitating substantial amounts of energy to fuel factories, offices, and other infrastructures. The demand for energy is projected to escalate in the forthcoming years. Hence, it is imperative to explore high performance and suitable materials for electrochemical energy storage systems. Lithium-ion batteries are becoming popular as a preferred option for portable electronic devices because they offer rechargeability, relatively long lifespan with high energy density. There are some shortcomings such as safety concerns for thermal runways, and fires caused by overheating, toxic heavy metals containing cathode materials, scarcity of raw Li etc., making its use difficult for electronic devices.[1] Hence, researchers and manufacturers are exploring alternatives, such as lithium-sulfur (Li-S) batteries, solid-state batteries, and flow batteries to develop safer and more sustainable solutions for storing energy. Due to high theoretical energy density ($\sim 2600 \text{ Wh Kg}^{-1}$) and non-toxicity, Li-S batteries have arisen as promising battery systems. Additionally, sulfur is an abundant and low-cost material, which could potentially reduce the cost of Li-S batteries.[2-5] Nevertheless, there are some technical hurdles yet to be overcome before Lithium-Sulfur (Li-S) batteries can be extensively used, including low cyclic efficiency, poor conductivity, shuttle effect, and a significant volumetric change in sulfuric content.[6-8] We are principally concerned with the major issue of suppressing the shuttle effect. One crucial step is to stop the dissolution of lithium polysulfide into the electrolyte that further renders the battery dead. To tackle this limitation, scientists have been looking for host

materials that can bind to trap polysulfides, preventing their dissolution into the electrolyte and elevating battery performance.[9-14] A plethora of works have posited several materials and concepts as viable suppressors of the shuttle effect, including S and O-based functionalized MXene, many-body effect, and layered double hydroxide.[10-13] While the carbon 2-D stacked material boasts superior electron transportation, it exhibits a lack of efficacy in capturing lithium polysulfide and demonstrates low AE. Even after structural morphology changes carbon materials still face problems in establishing a secure effective bond with polysulfide. Recent investigations have explored layered double hydroxide (LDH) as a potential material for use as host material in Li-S batteries as they provide more surface area and strong binding affinity with polysulfides.[15-16] LDH, also known as ionic clay, boasts a wide range of applications, promising AE, and electrocatalytic properties, distinguishing it from other host materials. However, intense investigation on the LDH materials as host materials for the Li-S battery is yet to be explored. LDH powers can easily exfoliate monolayer on the substrate with a thickness of 0.48 nm and act as a barrier for polysulfide to dissolve into electrolyte.[17-22] LDH has certain advantages like intercalation, surface modification, and hybridization with noble and rare earth elements that can replace one metal (M^{2+}/M^{3+}) component with a new metal component. The reason behind choosing LDH is strong adsorption energy (AE), dual metal electrocatalytic different customizable nanostructures.[16] However, exploring a large number of possible LDH materials as a host material for Li-S battery through conventional DFT calculation is highly time demanding process.[23-27] Thus, machine learning (ML), known for its ultrafast refining of cathode host materials in a concise time with minimum computational cost can be used as a tool to overcome these limitations.[28-31]

Here, we have considered 74 sulfur host cathode materials and 6 lithium polysulfides having overall, 444 possible systems for this study. Among

all the possibilities, we have selected well sampled 61 materials and performed ML classification. By using trained best fitted model on complete set, we screen the stable LDH monolayer having optimum AE required to be suitable sulfur host cathode material for Li-S battery to prevent the shuttle effect. We have set a minimum threshold of -1 eV for the adsorption energy criterion in selecting an effective sulfur cathode host material.[31] The Gradient Boosting Classifier (GBC) and AdaBoost Classifier (ABC) were shown to be the best model fits for Class A and B, with an average accuracy of 89% and 92.75%, respectively. After that, we combine both sets and refine all possible stable LDH materials which bind with all polysulfides effectively. Further DFT has been carried out on the ML screened LDH materials to validate the ML predicted result. The flowchart of the work has been provided in Figure 1.1.

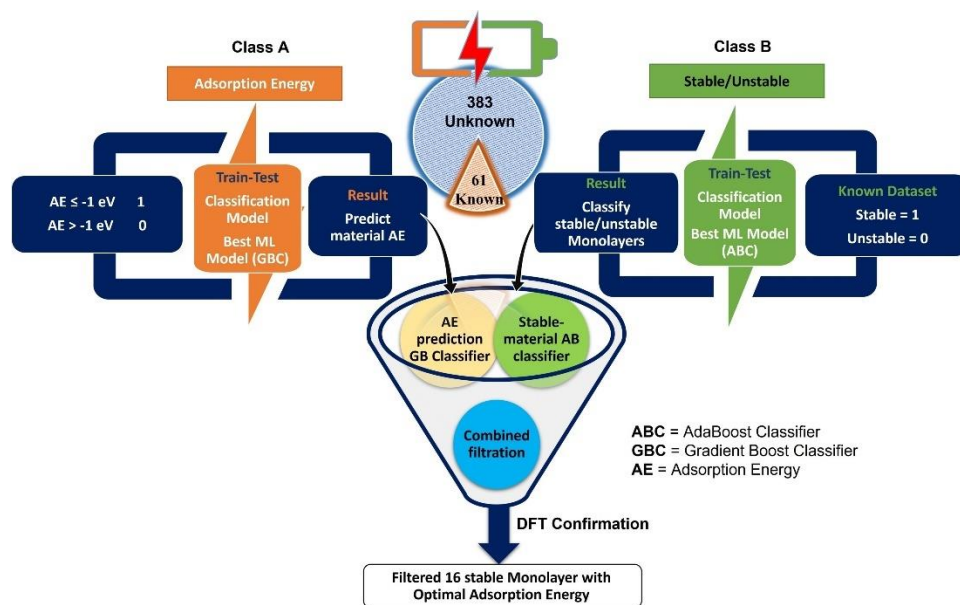


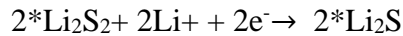
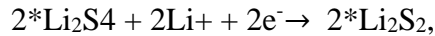
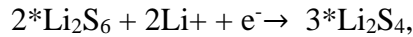
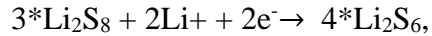
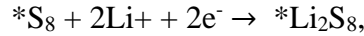
Figure 1.1: The flowchart of the work.

1.1. Lithium Sulfur Battery

The Li-S battery operates through an intricate electrochemical process that involves the synergistic interaction between lithium metal and sulfur, culminating in the creation of lithium sulfide (Li_2S) as the ultimate

discharge byproduct. As the battery discharges, lithium ions undergo oxidation at the anode, followed by their combination with sulfur, leading to the formation of lithium polysulfides. These ions and polysulfides then traverse the electrolyte to reach the cathode, where the polysulfides undergo reduction, resulting in their transformation into Li_2S and deposition of sulfur onto the cathode's surface. However, the emergence of lithium polysulfides during the discharge process of Li-S battery can give rise to their solubility in the electrolyte and consequent interaction with the solvent molecules, leading to potential issues with battery performance and stability. Given below is the demonstrated step-by-step mechanism of reaction for the Li-S battery.[8]

Li-S battery electrochemical reaction



1.2. Layer Double Hydroxide (LDH)

The LDH hydroxalcalite-like compound, which acts as the cathode host material, has a general formula $[M^{2+}_{1-x} M^{3+}_x (OH)_2]^{a+} \cdot [A_{a/n}]^{n-} \cdot yH_2O$, where M^{2+} is divalent cation and M^{3+} is trivalent cation, occupying the centre of octahedral sites in hydroxide layers.[15,16] Recent studies have demonstrated that 1,3-dioxolane (DOL) and 1,2-dimethoxyethane (DME) exhibit weak adsorption of lithium polysulfides, whereas carbon-based materials are incapable of effectively capturing them. To curb the shuttle effect and ensure efficient polysulfide retention, adsorption energy exceeding that of DOL and DME (-0.83 and -0.99 eV, respectively) is

required. As carbon-based materials display feeble adsorption properties, a minimum adsorption energy of -1.0 eV is needed to effectively capture polysulfides. Accordingly, class A is classified into materials with strong and weak binding energies based on this criterion. Total of 8 divalent cations M^{+2} (Ca^{+2} , Mg^{+2} , Mn^{+2} , Fe^{+2} , Co^{+2} , Ni^{+2} , Cu^{+2} , Zn^{+2}) and 5 trivalent cations M^{+3} (Al^{+3} , Ni^{+3} , Ti^{+3} , Co^{+3} , Fe^{+3}) were studied. Our decision to select this material stems from the wide range of functionalization possibilities it offers, as well as its ability to exhibit high adsorption energy with Li-S batteries. It is observed that presence of hydroxyl groups adsorbs strongly with polysulfides, further amplifying its efficacy.

1.3. Artificial Intelligence (AI)

AI systems leverage a blend of algorithms, machine learning, and deep learning to effectively handle vast quantities of data and detect patterns. Such systems are engineered to progressively enhance their performance, by learning from their experiences and refining their algorithms to augment their accuracy and efficiency. In the year 1950, the erudite British mathematician, Alan Turing, published a seminal paper entitled "Computing Machinery and Intelligence," in which a momentous concept was introduced, the Turing test. In contemporary times, Artificial Intelligence (AI) is progressively being utilized to mechanize monotonous tasks, scrutinize intricate data sets, and prognosticate and endorse solutions founded on patterns perceived in the data. As AI technology advances, it carries the potential to revolutionize almost every facet of our existence, starting from the way we communicate and work to the means by which we avail ourselves of healthcare and transportation. ML (Machine Learning) and DL (Deep Learning) are both subfields of AI (Artificial Intelligence) on the other hand DL is a more specialized form of Machine Learning that involves training neural networks with large amounts of data to recognize patterns and make predictions (Figure 1.2).

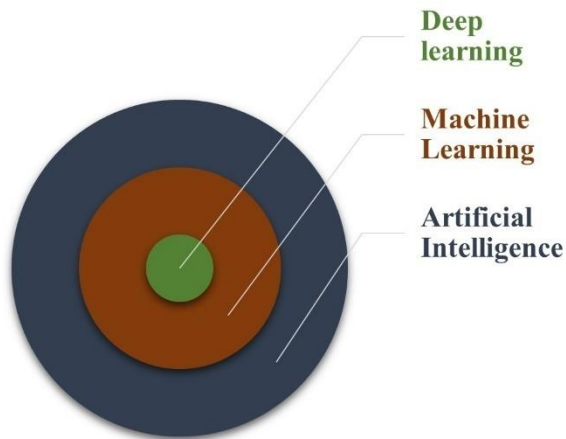


Figure 1.2: The depiction of the domain comprising DL, ML, and AI.

1.3.1. Machine Learning (ML)

Machine Learning (ML) is a specialized domain within the wider field of Artificial Intelligence (AI) that concentrates on the creation of intricate algorithms and statistical models that empower computer systems to process data, detect patterns, and make decisions without the need for explicit programming. These algorithms are engineered to scrutinize vast volumes of data and progressively enhance their accuracy and predictive capabilities over time. ML is a subset of both statistics and computer science, as it involves the use of statistical methods and algorithms from computer science to develop models that can learn from data. While AI and data science encompass broader areas that include machine learning as one of the components or techniques used in their applications.

Using the game of checkers by Arthur Samuel, published in 1959, is a pioneering paper in the machine learning field. Samuel took help of a self-learning program to play checkers and demonstrated the potential of machine learning to make decisions based on experience and improve over time. ML (Machine Learning) algorithms are further categorized into 3

main parts: supervised learning, unsupervised learning, and reinforcement learning. There can also be a fourth category, known as semi-supervised learning.

1.3.1.1. Supervised Learning

Supervised machine learning is an effective methodology for addressing problems that can be solved using labeled data. By leveraging labeled data, the model can learn patterns and establish relationships that enable it to make precise predictions on new, previously unseen data. Supervised machine learning has found application in diverse fields, including materials science where it excels in predicting the molecular adsorption energy on surfaces. In context of batteries, accurate projections of adsorption energies are pivotal in developing materials with improved performance characteristics. Researchers work on supervised machine learning to predict the adsorption energies for battery cathode materials. By training a model on labeled data of previously calculated adsorption energies, the model can learn to make accurate predictions for new, unseen cathode materials.

1.3.1.1.1. Classification

Classification is a sub-class of supervised machine learning algorithm that speculates class or category of a given input data point based on its features or attributes. Classification can be used for both binary classifications, where the goal is to predict one of two possible classes, and multi-class classification, where there are more than two possible classes. Here we used binary classification for our study to demonstrate the potential of machine learning techniques using multiple classification algorithms, for predicting the compatibility of materials for battery electrodes. These techniques could be useful in accelerating the research of new battery materials, ultimately leading to the discovery and production of more efficient and high-performance batteries.

1.3.1.2. ML models

- **Logistic Regression:** It is a classification algorithm that predicts the probability of an instance belonging to a specific class. It uses a sigmoid function to estimate the probability based on the output of a linear regression function, hence the name "logistic regression". Given below is the general equation of logistic regression (1.1).

$$\circ \sigma(t) = \frac{1}{1+e^{-t}} \tag{1.1}$$

- **Multilayer Perceptron:** It is a type of neural network that comprises of multiple layers of fully connected neurons. These layers are designed to transform input data into the desired output format. By combining neurons, the network can process complex input data and learn to make predictions or classifications. A schematic diagram of a Multi-Layer Perceptron (MLP) is depicted below figure 1.3. Multilayer Perceptron is a type of neural network that consists of multiple layers of fully connected neurons. These layers are designed to transform input data into the desired output format. By combining neurons, the network can process complex input data and learn to make predictions or classifications. Multi-Layer Perceptron (MLP) is depicted diagrammatically below Figure 1.3.

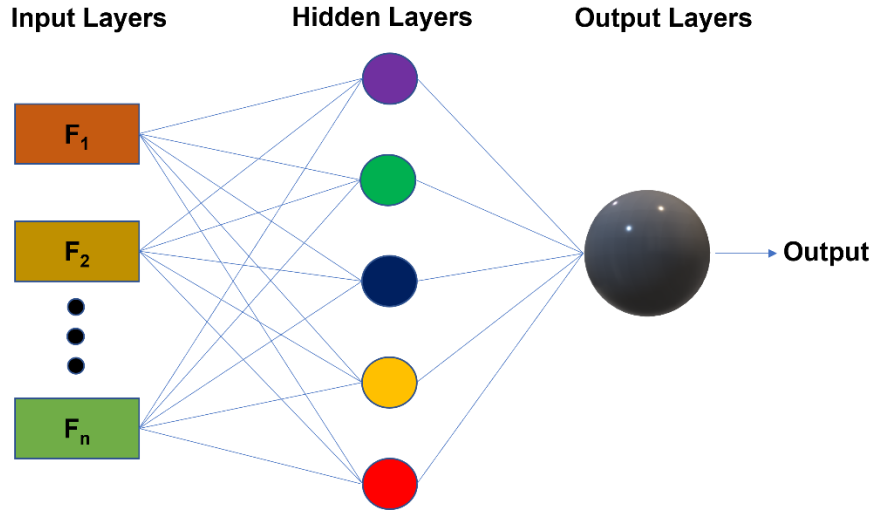


Figure 1.3: A schematic diagram of a Multi-Layer Perceptron (MLP).

- **Gaussian Naïve Bayes:** The Gaussian model assumes that input features are continuous and normally distributed. This model estimates the mean and variance of the distribution, which can be used to calculate probability density function (PDF) of input features. However, this assumption may not always hold true, especially if the data is skewed or has outliers. Where, $P(c)$ signify the probability function of gaussian naïve bayes (1.2).

$$P(c) = \frac{1}{\sqrt{2\pi\sigma_c^2}} e^{-\frac{(x-\mu_c)^2}{2\sigma_c^2}}$$

(1.2)

- **Bernoulli Naïve Bayes:** It is a binary classification algorithm that assumes the input features are binary. It models the probability of each feature given the class variable using a Bernoulli distribution and computes the prior probability of each class based on frequency of each class in training data. To make a prediction, it evaluates the posterior probability of each class given input features applying Bayes' theorem and chooses class with highest probability as predicted class. Bernoulli Naive Bayes is commonly used in text classification tasks.

- Perceptron:** Perceptron classification is a linear binary classification algorithm that learns a decision boundary separating two classes by iteratively updating weights of input features. Perceptron is linear binary classification algorithm that iteratively updates weights of input features to learn a decision boundary separating two classes. It computes dot product of weights and input features and applies a step function to the result. If output is incorrect, weights are adjusted in direction of misclassification. Given below presents a visual representation of a perceptron. (Figure 1.4)

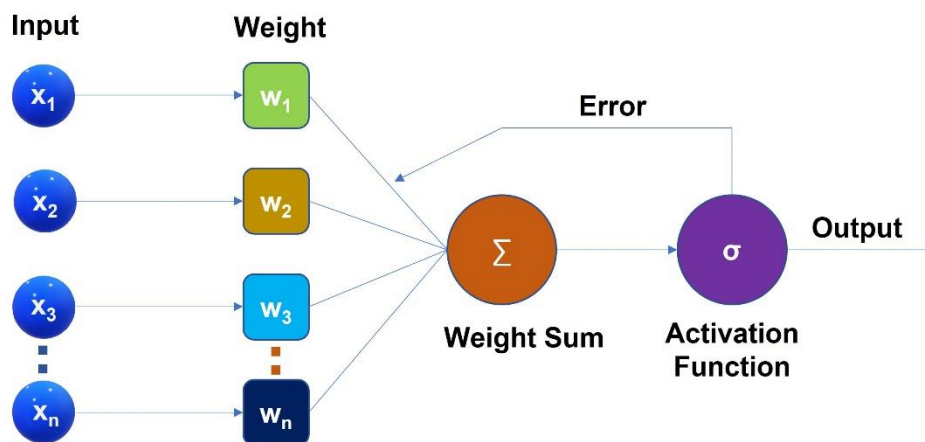


Figure 1.4: A visual representation of a perceptron.

- Stochastic Gradient Descent (SGD):** SGD Classifier is a linear binary classification algorithm that uses Stochastic Gradient Descent (SGD) optimization to update the weights of input features. It works by arbitrarily selecting a small batch of training examples for each iteration and updating the weights based on the gradient of loss function with respect to the weights. Advantage of SGD is that it converges faster than Gradient Descent and is more efficient for large datasets. However, it can be more sensitive to noise and may require more iterations to converge to the optimal solution. Here, θ_j denotes the parameters of the machine learning model being optimized.

$$\theta_j = \theta_j - \alpha \frac{\partial}{\partial \theta_j} \bar{J}(\theta)$$

(1.3)

- K-Nearest Neighbors (KNN):** is a non-parametric machine learning algorithm that utilizes distance metric to classify new instances by comparing them with the labeled instances in the training data. By finding the K nearest labeled instances, KNN allocates the class that is most common among them to the new instance. Hyperparameter K, the number of nearest neighbors, can be adjusted to fine-tune the model's accuracy. KNN is prevalent in diverse fields, including image classification, anomaly detection, and recommendation systems. There are several types of distance metrics used in KNN and other machine learning algorithms. Euclidean distance calculates the straight-line distance between two points in Euclidean space. Whereas Manhattan distance measures the distance between two points by adding the absolute differences of their coordinates. Minkowski distance is a more general distance metric that incorporates a parameter to regulate the "order" of the distance, which may be adjusted to calculate either the Euclidean or Manhattan distance.

$$\left(\sum_{i=1}^k (|x_i - y_i|)^q \right)^{1/q} \quad \text{--- Minikowski}$$

(1.4)

$$\sqrt{\sum_{i=1}^k (x_i - y_i)^2} \quad \text{--- Euclidean}$$

(1.5)

$$\sum_{i=1}^k |x_i - y_i| \quad \text{--- Manhattan}$$

(1.6)

- **Gradient Boosting Classifier (GBC):** Ensemble learning algorithm that combines weak prediction models to create a stronger model. The algorithm builds models sequentially, with each model improving on the errors of its predecessor. Gradient Boosting optimizes a loss function by iteratively adding new models to the ensemble, where each new model has been trained to diminish the residual errors of previous model as much as possible. The optimization is performed using gradient descent, hence the name "Gradient" Boosting. Final prediction is attained after combining predictions of every model in the ensemble. Gradient Boosting is popularly applied in both regression and classification problems and is known for its high accuracy and robustness against overfitting.
- **Decision Tree:** It is a powerful supervised learning algorithm that works on classification and regression tasks. It creates hierarchical model where each node corresponds to a feature, and each branch constitutes of a possible value or outcome of that feature. The algorithm recursively partitions the data by selecting the feature that maximizes information gain or minimizes impurities such as Gini impurity or entropy. The goal is to create a tree with high accuracy and low complexity which also extrapolates well to new data. To make predictions on new data, the input features are traversed through the branches of the tree until a leaf node is reached, which corresponds to the predicted outcome or class. Decision Trees are capable of handling both categorical and continuous features and are known for their interpretability. They can also handle missing values and outliers in the data. However, Decision Trees can be prone to overfitting and can be unstable when the data changes slightly. To mitigate these issues, techniques such as pruning and ensemble methods like Random Forests can be used. Given below shows the entropy and Gini formula.

$$Entropy = \sum_{i=1}^c -p_i \times \log_2 p_i \quad (1.7)$$

$$Gini = 1 - \sum_{i=1}^c p_i^2 \quad (1.8)$$

- **Xtreme Gradient Boosting (XG Boost):** XGBoost is a gradient boosting algorithm that uses regularization, parallel processing, and tree-pruning to reduce overfitting and improve performance. It builds decision trees iteratively and optimizes a loss function by adjusting the model's parameters based on the gradient and Hessian of the loss function. Final prediction is attained after combining the predictions of all trees in ensemble. XGBoost is popular algorithm for classification and regression tasks due to its speed, accuracy, and flexibility.
- **Random Forest Classifier (RFC):** Ensemble learning algorithm works by building multiple decision trees on subsets of training data and features, selected randomly. The algorithm aggregates the predictions of all the trees to make a final prediction, providing a more accurate and stable prediction than a single decision tree. Each decision tree is built independently, and the randomness introduced during the process reduces the risk of overfitting. Random Forest is commonly applied in classification and regression tasks, and its popularity is due to its high accuracy, interpretability, and ability to handle large datasets with many features.
- **Support Vector Classifier (SVC):** It is a supervised learning algorithm for classification and regression tasks, which forms a hyperplane or a set of hyperplanes in a high-dimensional space. The hyperplane is determined to have the maximum margin between classes, which is the distance between the hyperplane and closest data

points from each class. SVM is effective in handling high-dimensional data and can deal with non-linearly separable data by transforming the input space into a higher-dimensional space via kernel functions. SVM is operated in various areas such as image and text classification, and bioinformatics due to its efficiency and flexibility.

- **AdaBoost Classifier (ABC):** AdaBoost is an ensemble learning algorithm that combines multiple weak learners to form a stronger model. It functions by training weak learners sequentially, where each learner corrects the errors of its predecessor. The algorithm assigns weights to training examples based on their performance in previous iterations, with misclassified examples receiving higher weights.

The final model is an aggregation of all weak learners, weighed by their importance. AdaBoost is capable of handling high-dimensional data and can be exercised for classification, regression, and other prediction tasks. It has been employed in various fields, including computer vision, natural language processing, bioinformatics, and is known for its ability to improve the performance of weak learners. A flow diagram demonstrating the functionality of an Adaboost classifier is shown Figure 1.5.

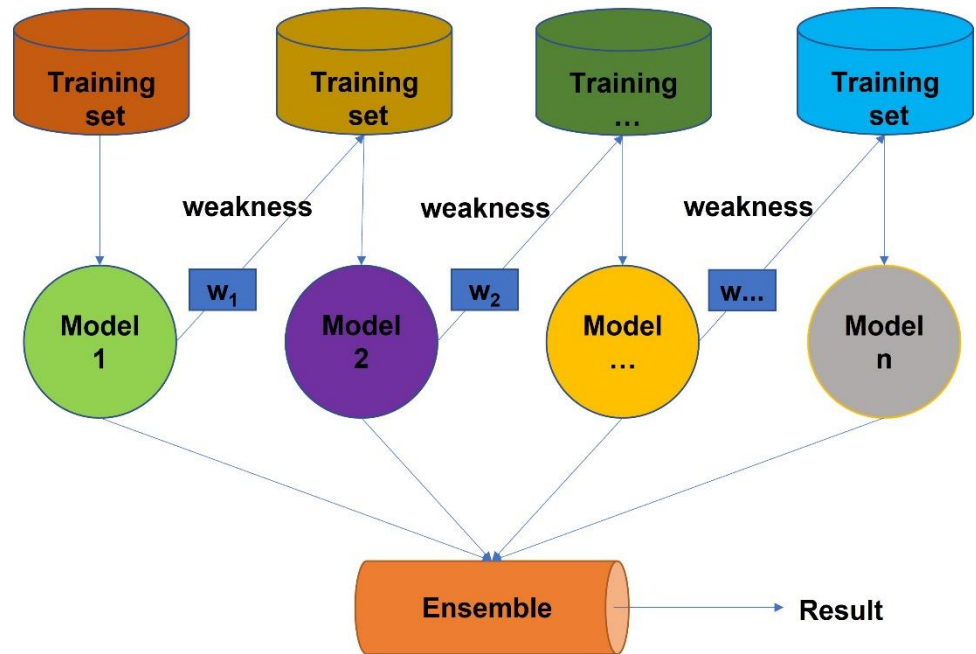


Figure 1.5: The working mechanism of an Adaboost classifier is depicted in a flowchart format.

- Linear Discriminant Analysis (LDA):** It is a supervised machine learning algorithm used for classification tasks. It analyzes the differences between classes and creates a linear combination of features that maximizes separation between them. The aim of LDA is projection of data onto a lower-dimensional space while preserving as much information as possible about the class labels. The algorithm calculates the mean and covariance matrix of each class and uses these statistics to determine the projection direction. LDA deduces the data to be normally distributed and that the classes have equal covariance matrices. LDA can also be helpful in dimensionality reduction and visualization.

1.3.1.3. Testing and Validation

In developing machine learning models for computational chemistry, testing and validation are crucial steps to ensure accurate predictions of chemical properties and behavior. Testing evaluates the model's performance on new data, while validation verifies its reliability and accuracy. These steps are necessary to identify any errors or limitations in the model.

1.3.1.4. Hyperparameter Tuning

Hyperparameter tuning is a process in machine learning that involves optimizing the settings of model parameters, known as hyperparameters, to improve the performance of the model. Hyperparameters are set prior to training the model and can significantly impact its accuracy. The process of hyperparameter tuning involves adjusting the values of hyperparameters and evaluating the resulting model performance. This is typically done through a combination of manual adjustments and automated methods such as grid search or Bayesian optimization. Proper hyperparameter tuning can help ensure that the model is performing optimally and can lead to better predictions in computational chemistry applications.

2. Computational Methods and Approximations

2.1. Many Body Schrödinger Equation

The Schrodinger equation is an essential equation that forms the basis of quantum mechanics. It is used to describe the behavior of particles, including electrons, within a quantum system. Specifically, Schrodinger equation (time-independent) has been valuable tool to calculate electronic structure in given molecules and materials. That equation is represented by:

$$H\psi = E\psi(r, R) \tag{2.1}$$

Here, H (Hamiltonian operator) contains information about the properties of the system, including its energy. The ψ symbol gives the wave function of system in consideration, which provides information regarding likelihood of finding a particle in a specific location. Finally, E denotes total energy of a given system. Using Hamiltonian operator of a quantum system, researchers can gain insight into the system's properties, such as its energy levels, momentum, and position. Additionally, the many body Schrödinger equation can be expressed as,

$$\begin{aligned}
H = & \frac{-\hbar^2}{2m_e} \sum_i \nabla_i^2 - \sum_I \frac{\hbar^2}{2M_I} + \frac{1}{2} \sum_{i \neq j} \frac{e^2}{|r_i - r_j|} \\
& + \frac{1}{2} \sum_{I \neq J} \frac{Z_I Z_J e^2}{|R_I - R_J|} - \sum_{i,I} \frac{Z_I e^2}{|r_i - R_I|}
\end{aligned}
\tag{2.2}$$

Here, \hbar -Planck's constant, i -imaginary unit. Solving the Schrodinger equation is a crucial tool in modern physics, particularly in the areas of quantum computing and materials science, as it allows researchers to make accurate predictions about the behavior of quantum systems. The many-body effect equation can be expressed in terms of interactions occurring between electrons and nuclei, as well as among nuclei themselves. Here, the first term denotes kinetic energy of electrons, which arises due to their motion within the electrostatic potential produced by the nuclei. Second term symbolizes the electron-nucleus potential energy and refers to the interactions among electrons and nuclei. Here, third term relates to repulsive energy between electrons, because of their negative charge causing repulsion. The fourth term refers to the attractive energy between nuclei and the electrons, because they carry opposite charges. The fifth and final term refers to the repulsive energy between nuclei in the system, which are positively charged and therefore repel each other. By incorporating all of these interactions, the many-body effect equation can accurately describe the behavior of particles in a complex electronic system and provide insights into their properties and behavior.

2.2. Born-Oppenheimer Approximation

The Born-Oppenheimer approximation is a theoretical concept that simplifies many-body Schrodinger equation by separating movement of electrons from positions of atomic nuclei. It is formulated on the basis of significant difference observed in mass between nuclei and electrons, where the latter can be considered stationary during the movement of electrons.[32] Thus, kinetic energy of nuclei has been neglected, and nuclear-nuclear Coulomb interaction is assumed to be constant.

$$H = \frac{-\hbar^2}{2m_e} \sum_i \nabla_i^2 + \frac{1}{2} \sum_{i \neq j} \frac{e^2}{|r_i - r_j|} + \frac{1}{2} \sum_{I \neq J} \frac{Z_I Z_J e^2}{|R_I - R_J|} - \sum_{i,I} \frac{Z_I e^2}{|r_i - R_I|} \quad (2.3)$$

By using this approximation, the many-body Schrodinger equation can be solved exclusively for electrons, while considering the nuclear-nuclear interactions explicitly. This simplification leads to a more practical solution reducing the complexity of problems. The Born-Oppenheimer approximation, also known as the clamped nuclei approximation, has been identified as a helpful tool in quantum chemistry.

2.3. Hartree-Fock Method

Hartree proposed a way to extend the mean-field approximation to describe the wavefunction of electron of an n-electron system by expressing it as product of one-electron wavefunctions, known as the Hartree product.[33] The wavefunction can be solved for each electron by considering the one-electron repulsion of only that electron and averaging the total interactions from all other electrons to create an average electrostatic field. This process is continued until a self-consistent

wavefunction is reached. However, this method is not taking into account the Pauli Exclusion Principle that requires total wavefunction to be antisymmetric when electrons exchange positions. This was resolved by Fock, who proposed using a determinant with the one-electron wavefunctions as elements to describe the electronic wavefunction of a system of two-electron system.

2.4. Density Functional Theory (DFT)

It is widely used in chemistry in order to understand the structure of electrons as well as properties of molecules and materials. It is a quantum mechanical method that utilizes the electron density of the system to compute various properties like energy, electronic structure, and reactivity, instead of the wavefunction. This approach is computationally less expensive compared to other methods.

In DFT, total energy of system is given as sum of kinetic energy (E_T), Coulombic interactions (E_J), electron-nuclear potential energy (E_V), and exchange/correlation energy (E_{XC}).

$$E^{DFT} = E_T + E_V + E_J + E_{XC} \quad (2.4)$$

The electronic density acts as the main variable in DFT, and all the terms in the energy equation except the kinetic energy depend on it. The orbitals in DFT are like molecular orbitals in Hartree-Fock theory. Development of DFT marks close relation with the work of P. C. Hohenberg and W. Kohn. These researchers proposed two crucial theorems that provided the basis for the theory. According to these theorems, the energy of ground state and electron density of system are solely determined by external potential acting on the system. DFT has revolutionized the approach to electronic structure calculations in chemistry, enabling the study of complex systems that were previously too computationally expensive to investigate.

$$\rho(r) = 2 \sum_i^{\text{orbitals}} |\psi_i(r)|^2 \quad (2.5)$$

2.4.1. Hohenberg-Kohn Theorems

The Hohenberg-Kohn Theorems play a crucial role in the developing Density Functional Theory (DFT); have significantly impacted the way chemists conduct electronic structure calculations. The First Theorem asserts that system's ground state properties can be distinctly resolved by ground state electronic density as a functional of the system.[34] This implies that if both the electron density and functional form are known, all the system properties can be obtained. However, the theorem does not provide any guidance on how to determine the functional density of electrons.

$$E = F(\rho(r)) \quad (2.6)$$

The Second Theorem of Hohenberg and Kohn asserts that true ground state electronic density corresponds to minimum energy of system. Energy obtained from any trial electronic density of system will be the upper bound estimation of true energy. [35] This theorem suggests using a variational approach where an initial guess of electronic density and corresponding energy is minimized iteratively until it reaches the exact electronic density of ground state and minimum energy within a convergence scale. This approach serves as a fundamental working principle of many self-consistent DFT-based codes.

$$E[\rho] \geq E_0[\rho_0(r)] \quad (2.7)$$

In second theorem of Hohenberg and Kohn, trial electron density and corresponding energy are denoted as ρ and E , respectively, while the true ground state electronic density and system's energy are represented as ρ_0 and E_0 .

2.4.2. Kohn-Sham Formulation

W. Kohn and L. J. Sham formulated a new approach which applies the Hohenberg-Kohn theorems, simplifying the many-body problem into non-interacting particle problem. This is achieved by defining each single particle with an effective potential, known as the Kohn-Sham potential. Total energy of ground state is stated as a function of Kohn-Sham orbitals and their associated density.

$$E[\rho(r)] = T_0[\rho(r)] + \frac{1}{2} \iint \frac{\rho(r)\rho(r')}{|r-r'|} dr dr' + \int V_{ext}(r)\rho(r)dr + E_{xc}[\rho(r)]dr + E_{II} \quad (2.8)$$

The energy comprises several terms that describe kinetic energy of non-interacting electrons, electron-electron Coulomb interaction, interaction between core and valence electrons, exchange-correlation interaction, and the nuclei-nuclei interaction.

The effective potential, containing external potential, Coulomb interaction, and exchange-correlation interaction, can be determined by knowing exchange-correlation potential. However, exchange-correlation interaction has proven to be a challenge to solve exactly, and therefore various approximations are used for simulating molecular and solid-state problems. [36,37]

2.4.3. Local Density Approximation (LDA)

LDA is drafted on the assumption that exchange-correlation energy of system is approximated by exchange-correlation energy of a homogenous electron gas with same electronic density. [37-39] The functional that describes exchange-correlation energy within local density approximation (LDA) is represented by,

$$E_{XC}^{LDA} = -\frac{3}{4} \left(\frac{3}{\pi}\right)^{1/3} \int \rho(r)^{4/3} dr \quad (2.9)$$

where $p(r)$ represents the electron density of such a system. This approximation is valid for systems with slowly varying electron densities, such as solids. However, for molecules, the electron density varies significantly, leading to inaccurate predictions of properties of molecules such as dissociation energy, bond-lengths, and electron distribution. Hence, LDA is often replaced by more accurate approximations, such as the Generalized Gradient Approximation (GGA) or hybrid functionals, which comprises of a fraction of exact exchange. These higher accuracy approximations provide a more reliable description of molecular properties.

2.4.4. Generalized Gradient Approximation (GGA)

GGA (Generalized Gradient Approximation) is an exchange-correlation functional that is widely employed in density functional theory. GGA considers both electron density as well as gradient of the electron density. By including gradient term, GGA significantly mitigates the over binding error that occurs in LDA and offers more precise predictions for various molecular and solid-state properties. Several widely used GGA functionals include Perdew, Burke, and Ernzerhof (PBE), Perdew and Wang (PW91), PBEsol, and revised PBE (RPBE). These functionals have undergone extensive testing and are known to provide accurate results for a variety of systems. Due to its ability to deliver accurate and reliable predictions while remaining computationally efficient, GGA has emerged as the most commonly used exchange-correlation functional. [41-43]

2.5. Basic Sets

"Basic sets" is a term used in computational chemistry to describe a collection of mathematical functions combined in a linear combination to approximate the wavefunction of an atom or molecule in quantum mechanical calculations. The complexity of basic sets can vary from minimal basis sets to double- and triple-zeta basis sets. It is important to

choose the right basic set as it can significantly affect the accuracy of the results obtained. Different basic sets are more suitable in case of different types of molecules or chemical reactions, but choosing the appropriate basic set is a critical aspect of designing a computational study.

2.5.1. Projector Augmented Wave (PAW) Method

In computational chemistry, wavefunctions near the atomic core exhibit a discontinuous nature, which requires plane waves in large numbers to describe the core electrons accurately. This results in noticeable increase in cost of computation of simulations of periodic systems. However, for many chemically and physically relevant problems, the valence electrons are the most significant contributors to material properties. Due to which plane-wave basis functions can be selectively employed to describe only the valence electrons. An effective potential, known as a pseudopotential, is a method that helps in expressing the interactions of core electrons and nuclei, [44] a method also referred to as the frozen-core approximation. There are various types of pseudopotentials, such as norm-conserving pseudopotentials and ultrasoft pseudopotentials (USPP), which differ in their energy cutoff and can be utilized in plane-wave based DFT calculations.

To reduce the dependency on empirical parameters for constructing pseudopotentials, Bloch proposed projector augmented wave (PAW) method, but Kresse and Joubert imposed it. The PAW method smooths the oscillating wavefunction between core and valence region by introducing a linear transformation. This is achieved by representing the all-electron function as a combination of the pseudo wavefunction, all-electron plane waves, pseudo plane waves, and a projector p' . As a result, the PAW method enhances the transferability of pseudopotentials and improves computational efficiency while reproducing results in agreement with all-electron calculations. In this thesis work, we utilize the PAW method

{implemented in Vienna ab-initio simulation package (VASP)} for working out calculations on periodic systems.

2.6. GPAW and ASE

GPAW and ASE are Python-based software packages used in material science and computational chemistry. GPAW is an electronic structure code that takes help from the projector augmented wave (PAW) method in order to deduce Kohn-Sham equations of density functional theory (DFT). ASE is toolkit that provides a wide range of modules and tools to interface with GPAW and other electronic structure codes, enabling users to perform a variety of computational tasks such as geometry optimization, molecular dynamics, and analysis of simulation results. Both GPAW and ASE are open-source and actively maintained by the scientific community. [45]

2.7. DFT Computations

The computations were executed through the utilization of Density Functional Theory (DFT) by means of the Vienna Ab initio Simulation Package (VASP) with the Perdew-Burke-Ernzerhof (PBE) functional predicated upon the generalized Gradient approximation (GGA) in case of electronic property and geometry optimization analyses.[46-48] The interactions taking place between ion cores and valence electrons were addressed through projector augmented wave (PAW) method.[49,50] Total energy was determined with great accuracy to a precision of 10^{-5} eV, while plane wave cut-off energy was fixed at 470 eV. Atomic structures were meticulously optimized by thoroughly relaxing the atomic positions till the value of force (Hellmann-Feynman) on all atoms was < 0.01 eV \AA^{-1} . Prior to being bound with lithium polysulfides, all LDH materials were optimized. Each slab adsorption structure, which was situated above 15 \AA in the Z-direction, was incorporated by vacuum layer to preclude potential layer-layer interactions. The DFT-D3 method was helpful in taking into

account the van der Waals interactions accurately. [51] Equation that computes the adsorption energy of the host material is presented below.

$$AE = E_{host} + E_{polysulfide} - E_{host+polysulfide} \quad (2.10)$$

It should be noted that the symbol E_{host} refers to the potential energy of an isolated LDH material layer without any substances present. On the other hand, the symbol $E_{polysulfide}$ represents the energy of the polysulfide, while $E_{host+polysulfide}$ gives optimized energy of entire system after the polysulfide has been bound. It is to be noted that the negative value of AE indicates the successful anchorage of the host material. Additionally, it is worth observing that the more negative the AE, the more potent the adsorption energy that exists between the cathode host material and host material and polysulfide.

3. Results and Discussion

3.1. Materials selection

Here, we have considered a monolayer of LDH with two distinct types. One of these types comprises 20 divalent metal cations and 4 trivalent metal cations, which are located at the center of octahedral sites and surrounded by 48 hydroxyl groups. Another contains 16 divalent metal cations and 12 trivalent metal cations which are situated in the center of the 56 hydroxyl groups arranged in a closed-packed structure. The top and side view of $[M^{+2}_{20}M^{+3}_4(OH)_{48}]$ -LDH and $[M^{+2}_{16}M^{+3}_{12}(OH)_{56}]$ -LDH material is provided in two distinct types are shown in Figure 3.1. We drop out the material having common divalent and trivalent cations. So, we left with 37 materials of each type A and B makes a total of 74 LDH materials. For our research, we extensively examined the complete range of polysulfide species (S_8 , Li_2S_8 , Li_2S_6 , Li_2S_4 , Li_2S_2 , and Li_2S). In total, we scrutinized 74 LDH materials with all possible lithium polysulfides, resulting in 444 sets of possibilities for calculating adsorption energy. Out of these, we selected 61 random sets for training and testing our sophisticated machine learning (ML) model and whole datasets were used into two distinct classes based on their different output. Class A involved predicting the adsorption energy of a material with 14 features, while class B contained information about the disintegration of the monolayer after anchoring, also comprising 14 features.

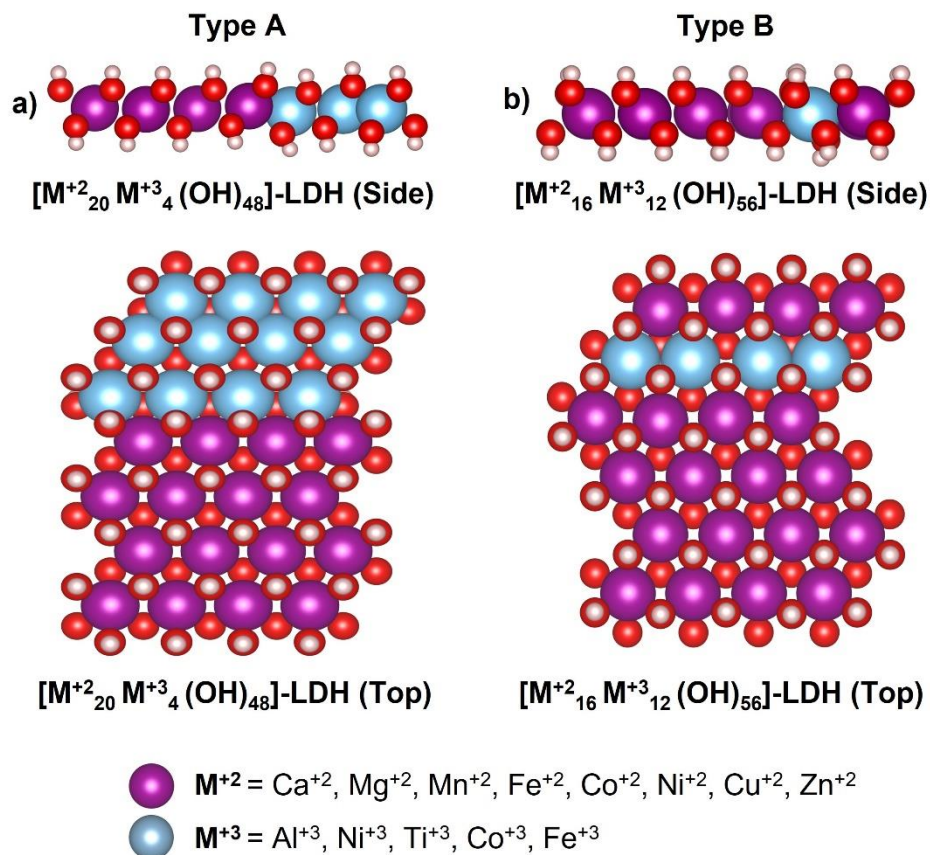


Figure 3.1: Illustrating the top and side views of two distinct types of LDH material.

We have examined the adsorption of complete range of polysulfide (S₈, Li₂S₈, Li₂S₆, Li₂S₄, Li₂S₂, and Li₂S) on LDH. In total, we scrutinized 74 LDH materials with all possible lithium polysulfides, resulting in 444 sets of possibilities for classifying the adsorption energy. The adsorption configuration of all the considered lithium-polysulfides on a sample LDH material ([Mg₂₀Al₄(OH)₄₈]) has been shown in Figure 3.2.

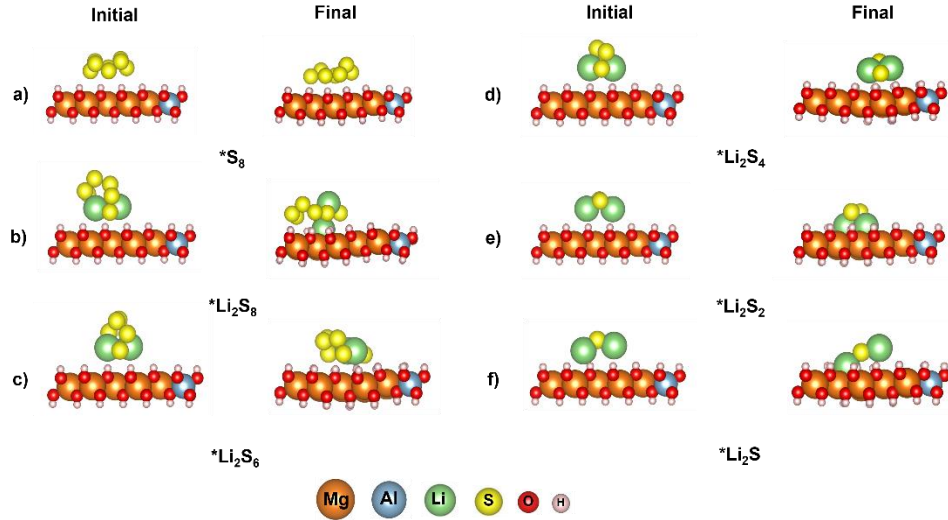


Figure 3.2: Adsorption configuration of lithium-polysulfides on $[\text{Mg}_{20}\text{Al}_4(\text{OH})_{48}]$ -LDH host material.

Ensuring the stability of the host material throughout the complete charge and discharge process is of paramount importance as it directly impacts the material's performance and cycle life in electrochemical energy storage devices. While optimizing monolayers, it was observed that certain materials exhibited instability, some monolayers disintegrating during the empty stage and others after adsorbing the polysulfides. The monolayers that disintegrated prior to anchoring were classified as unstable monolayers, such as (5CuCo, 5CuNi, 4Ca3Al, 4Ni3Al)-LDH, etc. Conversely, the monolayers that disintegrated after adsorbing the polysulfides proved challenging to restore also classified as unstable monolayer, such as (5MnAl, 5NiFe, 5NiCo, 5FeNi)-LDH, etc. To classify the disintegration/intact of LDH monolayers, we have created a new class, termed class B. LDH materials consist of cations with ionic radii similar to that of Mg^{+2} (0.72 Å), which can be incorporated into a brucite-like layer of closed-packed OH groups to form the LDH structure.[32] Material containing Ca^{+2} (1 Å) having a slight large radius difference is found to be unstable in most of the LDH material which is confirmed by DFT and also perfectly predicted by machine learning except in the case of

[Ca₁₆Ti₁₂(OH)₅₆]-LDH. We observed that all monolayers are effective at capturing Li₂S, but they may disintegrate when in contact with other polysulfides (Li₂S₂, Li₂S₄, Li₂S₆, Li₂S₈, S₈). Therefore, Li₂S may not play a significant role in class B prediction. LDH materials containing hydroxyl groups readily bind to lithium polysulfides, and by placing the polysulfides at the top of the layer, we can calculate the adsorption energy. In most cases, the lithium atom strongly binds to the oxygen atom of the hydroxyl group, providing a stable bond. However, in some instances, sulfur may detach the hydrogen atom from the hydroxyl group.

3.2. Features Engineering

In this study, we considered the chemical elemental properties of a material as a means of selecting pertinent features. Prior reports have relied on descriptors to appraise the multifaceted performances of materials.[38,39] We have specifically examined the lattice parameters and molecular properties of materials and polysulfides, resulting in 18 distinct features (Table S1). Upon constructing a Pearson correlation coefficient (PCC) heat map for these 18 features (Figure A1), we eliminated highly correlated features having a correlation coefficient above 0.95. Following this analysis, we constructed Pearson correlation coefficient (PCC) heat map of 15 features shown in Figure 3.3. Thus, creating a set of features that is optimal for machine learning models.

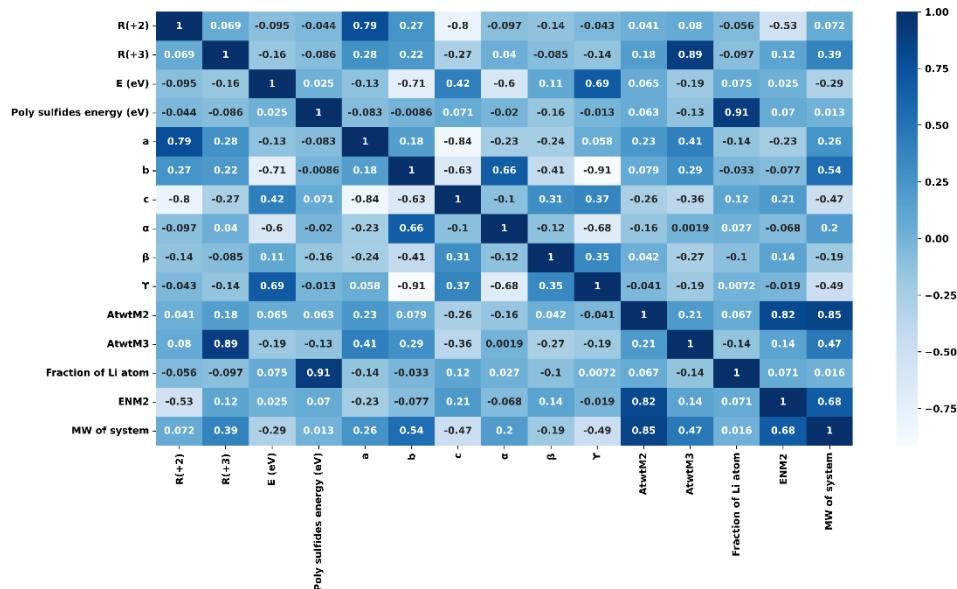


Figure 3.3: Pearson correlation coefficient (PCC) heat map of the considered features for this work.

In our feature selection process, we took into consideration 8 elemental properties, encompassing the likes of the atomic weight of divalent and trivalent cations, the radius of divalent and trivalent cations (M^{+2} and M^{+3}), the electronegativity of divalent cation (ENM2), the molecular weight of the system, the fraction of Lithium atom present, as well as the lattice parameters (a, b, c, α , β , and γ). We also included electronic properties, like optimized energy of the bereft LDH monolayer and polysulfide, to fully capture the material's properties. Table A1 shows the list of 15 features that were taken for this study.

3.3. Host material prediction via ML classification

We selected 61 well sampled materials covering adsorption of all the possible polysulfides and LDH for training and testing our sophisticated machine learning (ML) model. The whole dataset has been used into two distinct classification criteria based on their different output. Class A involved the identification of suitable sulfur host cathode materials based on the optimum adsorption energy criteria while class B contained

information about the disintegration of the monolayer after anchoring. These datasets were studied into two distinct forms classified as classes A and B. Class A focused on adsorption energy, categorized as either 0 ($AE > -1eV$) or 1 ($AE < -1eV$), while the class B contained data on LDH monolayer disintegration, classified as either 0 (monolayer disintegrates either before or after adsorption) or 1 (monolayer remains intact even after adsorption with polysulfide). Effective feature engineering was necessary to achieve optimal performance in training machine learning models. Upon applying feature engineering to 18 features, only 15 features were deemed suitable and consequently utilized in both classes. A supervised ML approach was adopted using a classification method, and 14 ML models were evaluated to identify the optimal model. The selected models were trained and tested using four different techniques, as demonstrated in Table 3.1.

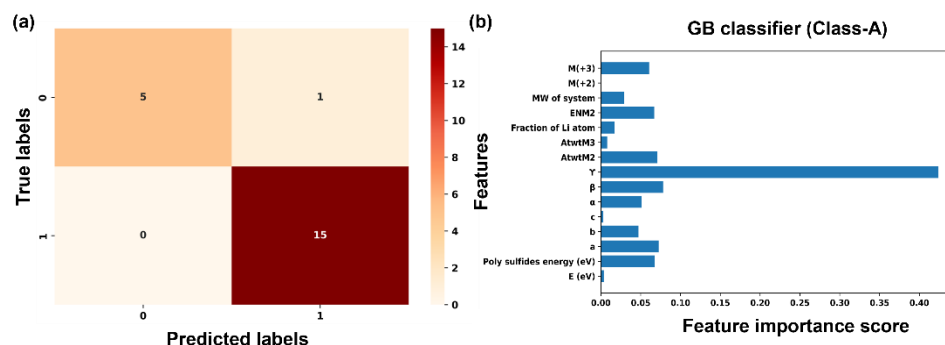
Table 3.1: Accuracy score of distinct models based on 4 different train and test split (Set-1, Set-2, Set-3, and Set-4).

Classification Model (Class A)	Set-1		Set-2		Set-3		Set-4	
	Train (48)	Test (13)	Train (45)	Test (16)	Train (42)	Test (19)	Train (40)	Test (21)
Logistic Regression	0.89	0.92	0.86	0.81	0.88	0.89	0.85	0.9
Multilayer perceptron (ANN)	0.72	0.53	0.88	0.87	0.57	0.78	0.6	0.71
Gaussian Naïve Bayes (NB)	0.85	0.46	0.75	0.87	0.78	0.68	0.72	0.76
Bernoulli Naïve Bayes (NB)	0.68	0.46	0.64	0.62	0.61	0.78	0.65	0.71
Perceptron (Linear Model)	0.68	0.46	0.35	0.37	0.42	0.21	0.40	0.28
Stochastic Gradient descent	0.68	0.46	0.64	0.62	0.42	0.21	0.60	0.71

K-Nearest Neighbors	0.79	0.84	0.75	1.00	0.76	0.84	0.70	0.80
Gradient Boosting	1.00	0.84	1.00	0.93	1.00	0.84	1.00	0.95
Decision Tree	1.00	0.84	1.00	0.87	1.00	0.78	1.00	0.85
XG-Boost	1.00	0.84	1.00	0.93	1.00	0.84	1.00	0.90
Random Forest	1.00	0.84	1.00	0.93	1.00	0.84	1.00	0.90
Support Vector	0.91	0.84	0.91	0.87	0.90	0.89	0.85	0.95
AdaBoost	1.00	0.76	1.00	0.93	1.00	0.78	1.00	0.90
Linear Discriminant Analysis	0.91	0.84	0.91	0.75	0.90	0.89	0.95	0.76

The datasets underwent training and testing at varying splits (48-13, 45-16, 42-19, 40-21). The resulting models utilized the given features and labels to classify the adsorption energy of LDH material, yielding varying levels of accuracy. In the case of Gradient Boosting Classifier (GBC), the model was trained and tested with a significant average accuracy of (100% and 89%) after considering all splits. We trained the model using set-4 with train test split of 66:33, having the highest training and testing accuracy of (100% and 95%), respectively. The model that achieved the highest accuracy consisted of 40 datasets for training and 21 datasets for testing. Using the GBC, a predictive model for the adsorption energy of the monolayer was established based on the obtained accuracy. The presented (Figure 3.4(a)) depicts a confusion matrix for a predicted dataset, indicating that the model correctly predicted the value of 0 on five instances and the value of 1 on fifteen instances. However, there was only one instance where the algorithm incorrectly predicted the value of 0 as 1. Moreover, during the training phase, feature importance scores were obtained implicitly, and the scores for each feature are provided (Figure 3.4(b)). The feature importance score is a valuable metric to assess the impact of a particular feature on the target variable. A higher score

denotes a stronger influence, making it more significant. It is noteworthy that the lattice parameter Υ has the most substantial impact on the training outcomes, as evidenced by its impressive f-score of 0.44. In contrast, the lattice parameters (a , b , α , and β), fraction of lithium atom, electronegativity of a divalent cation, radius of trivalent cation, radius of trivalent cation, and energy of a polysulfide having less impact than Υ but still possess noteworthy importance with moderate f-scores. The



remaining features have negligible influence.

Figure 3.4: (a) Confusion matrix of test dataset and (b) feature importance scores of the considered features for class-A classification.

The preservation of the cathode host material's structural integrity in batteries is a crucial consideration. Class B output is classified as either 0 or 1, representing the disintegration and non-disintegration of the monolayer, respectively. We employed 14 distinct supervised ML models, using a classification approach. The models underwent training and testing using the same methodology across multiple splits (48-13, 45-16, 42-19, 40-21). The accuracy of each model varied across different splits, as depicted in the accompanying (Table 3.2). In case of AdaBoost Classifier (ABC), the model was trained and tested with a remarkable average accuracy of (100 and 92.75) % after considering all splits. We trained the model using set-4 with train test split of (66:33) % stands out as the

preeminent model for classification, exhibiting unparalleled mastery with flawless training and testing accuracy of 100%.

Table 3.2: Accuracy score of various ML models for the classification of stable and unstable LDH materials on four distinct train and test splits.

Classification Model (Class B)	Set-1		Set-2		Set-3		Set-4	
	Train (48)	Test (13)	Train (45)	Test (16)	Train (48)	Test (13)	Train (45)	Test (16)
Logistic Regression	0.81	0.76	0.82	0.68	0.95	0.73	0.72	0.90
Multilayer perceptron (ANN)	0.79	0.69	0.77	0.75	0.80	0.73	0.77	0.76
Gaussian Naïve Bayes (NB)	0.81	0.76	0.84	0.68	0.80	0.78	0.75	0.90
Bernoulli Naïve Bayes (NB)	0.79	0.69	0.77	0.75	0.78	0.73	0.77	0.76
Perceptron (Linear Model)	0.79	0.69	0.77	0.75	0.78	0.73	0.77	0.76
Stochastic Gradient descent	0.68	0.53	0.22	0.25	0.28	0.26	0.77	0.76
K-Nearest Neighbors	0.72	0.76	0.88	0.93	0.80	0.73	0.72	0.80
Gradient Boosting	1.00	0.84	1.00	0.93	1.00	0.84	1.00	0.95
Decision Tree	1.00	0.84	1.00	0.68	1.00	0.84	1.00	0.90
XG-Boost	1.00	0.76	1.00	0.93	1.00	0.84	1.00	0.90
Random Forest	1.00	0.76	1.00	0.84	1.00	0.84	1.00	0.90
Support Vector	0.87	0.84	0.88	0.68	0.88	0.84	0.85	0.90
AdaBoost	1.00	0.84	1.00	0.93	1.00	0.94	1.00	1.00
Linear Discriminant Analysis	0.95	0.92	0.95	0.75	0.95	0.84	0.97	0.85

The best-fitted model comprises of well sampled 40 training datasets, while the remaining 21 datasets are used for testing. The correlation matrix (Figure 3.5(a)) indicates that the algorithm flawlessly predicted 5 times 0 and 16 times 1. The feature importance plot (Figure 3.5(b)) reveals that certain attributes, such as γ , β , a , and the divalent cation radius, have a considerably higher feature importance greater than 0.10. Conversely, some features, such as electronegativity of the divalent cation, energy of the host material without substance, and α , have negligible feature importance. Additionally, some attributes such as the radius of the trivalent cation, molecular weight of the system, fraction of lithium atom, atomic weight of divalent and trivalent cation, b , c , optimized energy of polysulfide, the radius of trivalent cation, and molecular weight of the system, have a moderate impact.

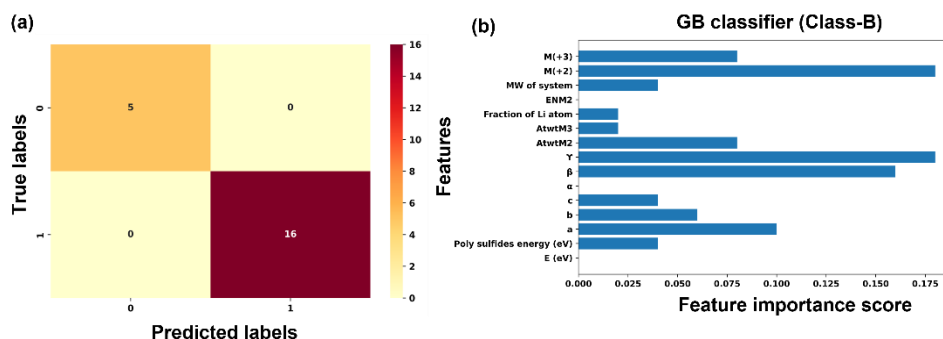


Figure 3.5: (a) Confusion matrix of test dataset and (b) feature importance scores of the considered features for class-B classification.

The optimized hyperparameters used to fit the GBC and ABC ML models for Class A and B have been provided in Table A2 and A3, respectively. Further, both models are cross verified by 10-fold cross-validation (CV) in which, the 61 datasets are partitioned into 10 equal-sized subsets randomly. Then, model is trained and evaluated 10 times, where each time, different subset is taken as test set, and other nine subsets are taken

to train the model. The results of the 10 iterations are then averaged to obtain estimate of performance of model on complete dataset. The advantage of using 10-fold cross-validation is that it produces better estimate of performance of model than a single train-test split, as it evaluates entire available data for both training and testing. Specifically, the arithmetic mean of the ten-fold cross-validation results indicate an 81% level of accuracy in testing for GBC for Class A which nearly matched with our average accuracy of model 89%, while ABC attains a 92% level of accuracy in cross-validation for Class B perfectly matched with our average accuracy of 92.75%. (Table 3.3)

Table 3.3: Mean accuracy for each fold of 10-fold cross-validation using GB-classifier for class A classification and AB-classifier for class B classification.

K fold	Class A	Class B	K fold	Class A	Class B
K-1	0.84	0.91	K-6	0.83	0.97
K-2	0.82	0.85	K-7	0.81	0.93
K-3	0.72	0.92	K-8	0.82	0.91
K-4	0.79	0.93	K-9	0.83	0.91
K-5	0.79	0.95	K-10	0.83	0.92
Mean Accuracy: Class A: 0.81; Class B: 0.92					

The Gradient Boosting ML model's predictions for 444 datasets regarding class A. Probability can effectively aid in identifying and selecting

materials that have a high likelihood of satisfying specific criteria. As a result, Gradient Boosting screened 29 cathode host materials that exhibit a probability greater than 0.99% and possess effective binding energy, making them promising candidates for further analysis. Furthermore, the predicted outcome for class B by the AdaBoost algorithm. To ensure high screening we filtered 44 intact LDH monolayers with a probability greater than 85%. Finally, we consolidate the cathode host materials predicted for both classes and conduct a screening process to identify the 22 most viable options. Due to the crucial role played by Li_2S_6 in Lithium Sulfur battery charge and discharge processes,[31] we used this species to validate the accuracy of predicted results obtained through Density Functional Theory (DFT) calculations on 22 refined Layered Double Hydroxide (LDH) monolayers. Our DFT analysis identified 16 of the LDH monolayers as optimal cathode host materials (Table 3.4) that can effectively mitigate the shuttle effect during battery cycling, indicating their high potential for practical application. Here, A and B refers the predicted outcome of ML model for class A and class B. Notably, these selected LDH monolayers exhibit a high degree of effective adsorption energy, enabling them to serve as a stable adsorption surface for all polysulfides. Cohesive energy greater than AE shows that our LDH material remains stable after adsorption which we can observe from Table 3.4.

Table 3.4: Predicted outcome by ML model with probability of getting 1 for each class and cross verified by DFT predicted AE.

S. NO.	Cathode host material	A	B	P _A (1)	P _B (1)	DFT result AE (eV)	Cohesive Energy (eV)
1	[Mg ₂₀ Al ₄ (OH) ₄₈]	1	1	0.9995	0.8518	-3.89	4.15
2	[Mg ₂₀ Fe ₄ (OH) ₄₈]	1	1	0.9986	0.8514	-1.96	4.07
3	[Fe ₁₆ Co ₁₂ (OH) ₅₆]	1	1	0.9922	0.9867	-5.22	2.62
4	[Mn ₁₆ Co ₁₂ (OH) ₅₆]	1	1	0.9984	0.9388	-2.98	3.95
5	[Ni ₁₆ Co ₁₂ (OH) ₅₆]	1	1	0.9997	0.9361	-1.21	3.92
6	[Co ₁₆ Ni ₁₂ (OH) ₅₆]	1	1	0.9998	0.9364	-2.16	3.92
7	[Fe ₁₆ Ni ₁₂ (OH) ₅₆]	1	1	0.9998	0.9650	-4.05	3.84
8	[Zn ₁₆ Ni ₁₂ (OH) ₅₆]	1	1	0.9995	0.8701	-2.08	3.67
9	[Mg ₁₆ Fe ₁₂ (OH) ₅₆]	1	1	0.9996	0.9855	-6.25	2.47
10	[Mn ₁₆ Fe ₁₂ (OH) ₅₆]	1	1	0.9991	0.9482	-1.88	3.93
11	[Ni ₁₆ Fe ₁₂ (OH) ₅₆]	1	1	0.9998	0.9459	-3.49	3.92
12	[Zn ₁₆ Fe ₁₂ (OH) ₅₆]	1	1	0.9998	0.9441	-6.59	3.69
13	[Ca ₁₆ Ti ₁₂ (OH) ₅₆]	1	1	0.9923	0.9433	-1.30	4.46
14	[Mg ₁₆ Ti ₁₂ (OH) ₅₆]	1	1	0.9991	0.9855	-4.42	4.29
15	[Mn ₁₆ Ti ₁₂ (OH) ₅₆]	1	1	0.9993	0.9758	-4.38	4.11
16	[Ni ₁₆ Ti ₁₂ (OH) ₅₆]	1	1	0.9994	0.9482	-4.49	4.18

4. Conclusion

Here, combined ML-DFT approach has been applied to screen out stable and suitable cathode host materials from two different classes of LDH monolayers for Li-S battery in order to minimize the shuttle effect. First, we have performed different classification algorithms for identifying cathode host materials having optimum adsorption energy criteria upon Li-S polysulfide adsorption. Among the applied algorithms Gradient Boosting model has been found to be the most suitable ML model for class A classification with 95% accuracy. On applying Gradient Boosting model, we have identified 29 materials having strong adsorption with polysulfides. Further, another classification has been performed to detect the stability of all the cathode host materials upon Li-S adsorption where AdaBoost classification model has shown 100% accuracy for the identification of stable cathode materials and leads us to 44 structurally stable cathode host LDH monolayers. Combining both Gradient Boosting and AdaBoost classifier models we have screened out 22 effective viable cathode host materials with strong adsorption energy along with structural integrity. Further, we have carried out DFT calculation on all 22 filtered LDH monolayers by adsorbing Li_2S_6 to validate the ML predicted result. Among the 22 LDH monolayers, 16 LDH monolayers have been found to be suitable host cathode materials from DFT result which can suppress the shuttle effect effectively. We have used ML models followed by DFT for the superfast screening of cathode host materials from a huge dataset (444)

for Li-S battery. We believe our combined ML-DFT approach will contribute to the experimental field by providing a right direction to the experimental researchers to design suitable cathode host materials which can suppress shuttle effect in Li-S battery.

Supporting Information

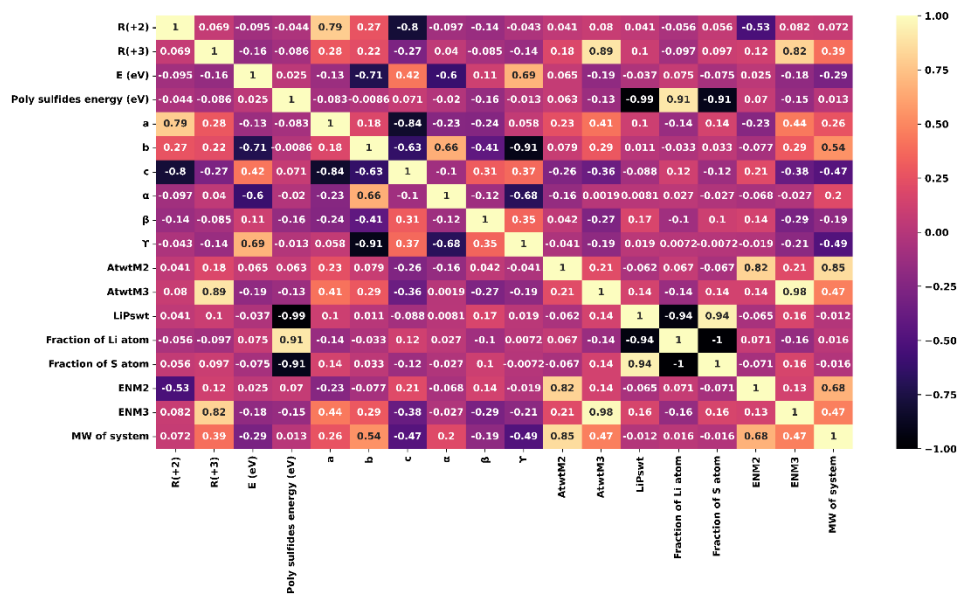


Figure A1: Pearson correlation coefficient (PCC) heat map plot considered before features engineering.

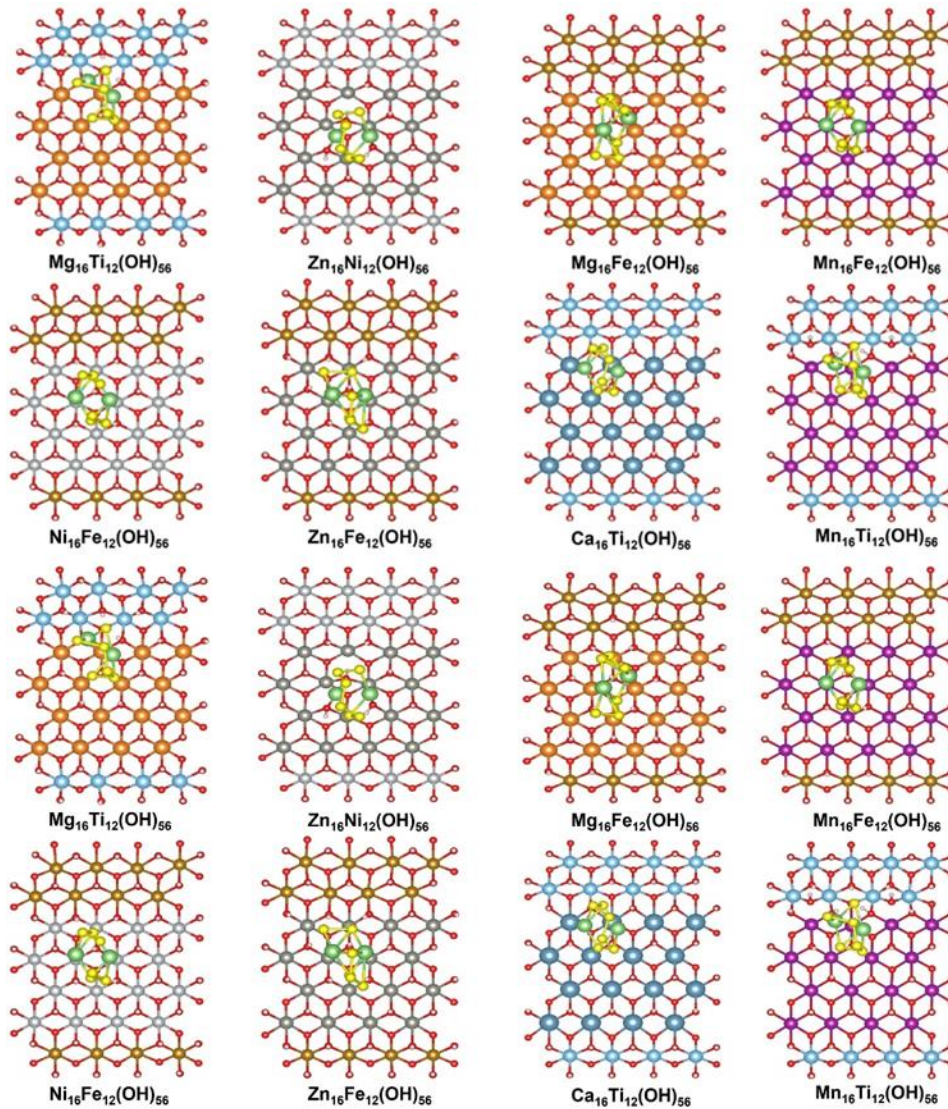


Figure A2: Optimized structures of Li_2S_6 adsorbed on 16 substrates.

Table A1: List of features that were used for the ML model. Abbreviations used in the manuscript to represent the features are given in parentheses.

1	Lattice parameter along x-axis (a)
2	Lattice parameter along y-axis (b)
3	Lattice parameter along z-axis (c)

4	Molecular weight of a material (MW of system)
5	Fraction of lithium present in lithium polysulfide intermediates (Fraction of Li atom)
6	Fraction of Sulfur present in lithium polysulfide intermediates (Fraction of S atom)
7	Electronegativity of divalent cation (ENM2)
8	Electronegativity of Trivalent cation (ENM3)
9	Polysulfide energy
10	Angle between y-z axis (α)
11	Angle between x-z axis (β)
12	Angle between y-x axis (γ)
13	Atomic weight of divalent cation (AtwtM2)
14	Atomic weight of trivalent cation (AtwtM3)
15	Molecular weight of lithium polysulfide intermediates (LiPswt)
16	Ionic radius of divalent cation (R(+2))
17	Ionic radius of trivalent cation (R(+3))
18	Optimized energy of bereft monolayer (E (eV))
19	Optimized energy of polysulfide (Polysulfide energy)

Table A2: Hyperparameter used in tuning the Gradient Boosting model.

Hyperparameter	Gradient Boosting
loss	Log_loss
n_estimators	friedman_mse
criterion	friedman_mse
min_samples_split	2
max_depth	3
Random_state	43

Table A3: Hyperparameter used in tuning the AdaBoost model.

Hyperparameter	AdaBoost
algorithm	SAMME.R
learning_rate	1
n_estimators	50

REFERENCES

- [1] Evers, S., Nazar, L. F. (2013), New approaches for high energy density lithium–sulfur battery cathodes, *Acc. Chem. Res.*, 46(5), 1135–1143 (DOI: 10.1021/ar3001348)
- [2] Ji, X., Lee, K., Nazar, L. F. (2009), A highly ordered nanostructured carbon–sulphur cathode for lithium–sulphur batteries. *Nat. Mater.*, 8(6), 500–506 (DOI: 10.1038/nmat2460)
- [3] Bruce, P. G., Freunberger, S., Hardwick, L. J., Tarascon, J. (2011b), Li–O₂ and Li–S batteries with high energy storage, *Nat. Mater.*, 11(1), 19–29 (DOI: 10.1038/nmat3191)
- [4] Manthiram, A., Fu, Y., Chung, S. H., Zu, C., Su, Y. (2014), Rechargeable Lithium–Sulfur Batteries, *Chem. Rev.*, 114(23), 11751–11787 (DOI: 10.1021/cr500062v)
- [5] Cui, J., Li, Z., Wang, G., Guo, J., Shao, M. (2020), Layered double hydroxides and their derivatives for lithium–sulfur batteries, *J. Mater. Chem. A, Materials for Energy and Sustainability*, 8(45), 23738–23755 (DOI: 10.1039/d0ta08573a)
- [6] Diao, Y., Xie, K., Matic, A., Hong, X. (2013), Shuttle phenomenon – The irreversible oxidation mechanism of sulfur active material in Li–S battery, *J. Power Sources*, 235, 181–186 (DOI: 10.1016/j.jpowsour.2013.01.132)
- [7] Zhang, S. (2013b), Liquid electrolyte lithium/sulfur battery: Fundamental chemistry, problems, and solutions, *J. Power Sources*, 231, 153–162 (DOI: 10.1016/j.jpowsour.2012.12.102)
- [8] Feng, S., Fu, Z., Chen, X., Zhang, Q. (2022), A review on theoretical models for lithium–sulfur battery cathodes. *InfoMat.*, 4(3) (DOI: 10.1002/inf2.12304)

- [9] Wang, L., Song, Y., Zhang, B., Liu, Y., Wang, Z., Li, G., Liu, S., Gao, X. (2020), Spherical metal oxides with high tap density as sulfur host to enhance cathode volumetric capacity for lithium–sulfur battery, *ACS Appl. Mater. Interfaces.*, 12(5), 5909–5919 (DOI: 10.1021/acsami.9b20111)
- [10] Gogotsi, Y., Pinilla, S. F., McEvoy, N., Cullen, C. P., Anasori, B., Long, E., Park, S. M., Seral-Ascaso, A., Shmeliov, A., Krishnan, D., Morant, C., Liu, X., Duesberg, G. S., Gogotsi, Y., Nicolosi, V. (2017b), Oxidation stability of colloidal two-dimensional titanium carbides (MXenes), *Chem. Mater.*, 29(11), 4848–4856 (DOI: 10.1021/acs.chemmater.7b00745)
- [11] Yao, C., Li, W., Duan, K., Zhu, C., Li, J., Ren, Q., Bai, G. (2021), Properties of S-functionalized nitrogen-based MXene (Ti₂NS₂) as a hosting material for lithium-sulfur batteries, *Nanomater.*, 11(10), 2478 (DOI: 10.3390/nano11102478)
- [12] Fang, M., Liu, X., Ren, J., Yang, S., Su, G., Fang, Q., Lai, J., Li, S., Liu, W. (2020), Revisiting the anchoring behavior in lithium-sulfur batteries: many-body effect on the suppression of shuttle effect, *Npj Comput. Mater.*, 6(1),8. (DOI:10.1038/s41524-020-0273-1)
- [13] Cao, D., Yin, C., Shi, D., Fu, Z., Zhang, J., Li, C. (2017), Cubic Perovskite Fluoride as Open Framework Cathode for Na-Ion Batteries, *Adv. Funct. Mater.*, 27(28), 1701130 (DOI: 10.1002/adfm.201701130)
- [14] Zhang, Q., Wang, Y., Seh, Z. W., Fu, Z., Zhang, R., Cui, Y. (2015), Understanding the anchoring effect of Two-Dimensional Layered Materials for Lithium–Sulfur Batteries, *Nano Lett.*, 15(6), 3780–3786 (DOI: 10.1021/acs.nanolett.5b00367)
- [15] Cui, J., Li, Z., Wang, G., Guo, J., Shao, M. (2020), Layered double hydroxides and their derivatives for lithium–sulfur batteries, *J. Mater. Chem. A, Materials for Energy and Sustainability*, 8(45), 23738–23755 (DOI: 10.1039/d0ta08573a)

- [16] Laipan, M., Yu, J., Li, Z., Smith, A., He, H., O'Hare, D., Sun, L. (2020), Functionalized layered double hydroxides for innovative applications, *Mater. Horiz.*, 7(3), 715–745 (DOI: 10.1039/c9mh01494b)
- [17] Chen, B., Zhang, Z., Kim, S., Lee, S., Lee, J., Kim, W. (2018), Ostwald ripening driven exfoliation to ultrathin layered double hydroxides nanosheets for enhanced oxygen evolution reaction, *ACS Appl. Mater. Interfaces.*, 10(51), 44518–44526 (DOI: 10.1021/acsami.8b16962)
- [18] Song, F., Hu, X. (2014), Exfoliation of layered double hydroxides for enhanced oxygen evolution catalysis, *Nat. Commun.*, 5(1) (DOI: 10.1038/ncomms5477)
- [19] Wang, Q., Chen, L., Guan, S., Zhang, X., Wang, B., Cao, X., Yu, Z. G., He, Y., Evans, D. M., Feng, J., Li, D. (2018), Ultrathin and vacancy-rich CoAl-Layered double hydroxide/graphite oxide catalysts: promotional effect of cobalt vacancies and oxygen vacancies in alcohol oxidation, *ACS Catal.*, 8(4), 3104–3115 (DOI: 10.1021/acscatal.7b03655)
- [20] Wang, Y., Zhang, Y., Liu, Z., Xie, C., Feng, S., Liu, D., Shao, M., Wang, S. (2017), Layered double hydroxide nanosheets with multiple vacancies obtained by dry exfoliation as highly efficient oxygen Evolution electrocatalysts, *Angew. Chem.*, 56(21), 5867–5871 (DOI: 10.1002/anie.201701477)
- [21] Liu, R., Wang, Y., Liu, D., Zou, Y., Wang, S. (2017), Water-Plasma-Enabled exfoliation of ultrathin layered double hydroxide nanosheets with multivacancies for water oxidation. *Adv. Mat.*, 29(30), 1701546 (DOI: 10.1002/adma.201701546)
- [22] Li, Z., Liu, K., Fan, K., Yang, Y., Shao, M., Wei, M., Duan, X. (2019), Active-Oxygen-Enhanced homogeneous nucleation of lithium metal on ultrathin layered double hydroxide, *Angew. Chem.*, 58(12), 3962–3966. (DOI: 10.1002/anie.201814705)
- [23] He, Q., Yu, B., Li, Z., Zhao, Y. (2019), Density functional theory for battery materials. *Energy Environ. Mater.*, 2(4), 264–279. (DOI: 10.1002/eem2.12056)

- [24] Jain, A., Shin, Y., Persson, K. A. (2016), Computational predictions of energy materials using density functional theory, *Nat. Rev. Mater.*, *1*(1), 15004 (DOI: 10.1038/natrevmats.2015.4)
- [25] Qiu, P., Yao, Y., Li, W., Sun, Y., Jiang, Z., Mei, B., Gu, L., Zhang, Q., Shang, T., Yu, X., Yang, J., Fang, Y., Zhu, G., Zhang, Z., Zhu, X., Zhao, T., Jiang, W., Fan, Y., Ma, B., Lui, L., Yu, Y., Luo, W. (2021), Sub-nanometric manganous oxide clusters in nitrogen doped mesoporous carbon nanosheets for high-performance lithium–sulfur batteries, *Nano Lett.*, *21*(1), 700–708 (DOI: 10.1021/acs.nanolett.0c04322)
- [26] Qiu, P., Yao, Y., Li, W., Sun, Y., Jiang, Z., Mei, B., Gu, L., Zhang, Q., Shang, T., Yu, X., Yang, J., Fang, Y., Zhu, G., Zhang, Z., Zhu, X., Zhao, T., Jiang, W., Fan, Y., Ma, B., Li, W. (2021), Sub-nanometric manganous oxide clusters in nitrogen doped mesoporous carbon nanosheets for high-performance lithium–sulfur batteries. *Nano Lett.*, *21*(1), 700–708 (DOI: 10.1021/acs.nanolett.0c04322)
- [27] Li, H., Ma, S., Cai, H., Zhou, H., Huang, Z., Hou, Z., Wu, J., Yang, W., Yi, H., Fu, C., Kuang, Y. (2018), Ultra-thin Fe₃C nanosheets promote the adsorption and conversion of polysulfides in lithium-sulfur batteries. *Energy Storage Mater.*, *18*, 338–348 (DOI: 10.1016/j.ensm.2018.08.016)
- [28] Joshi, R., Eickholt, J., Li, L., Fornari, M., Barone, V., Peralta, J. E. (2019), Machine learning the voltage of electrode materials in metal-ion batteries. *ACS Appl. Mater. Interfaces*, *11*(20), 18494–18503 (DOI: 10.1021/acsami.9b04933)
- [29] Wang, G., Fearn, T., Wang, T., Choy, K. (2021), Machine-Learning approach for predicting the discharging capacities of doped lithium nickel–cobalt–manganese cathode materials in li-Ion batteries *ACS Cent. Sci.*, *7*(9), 1551–1560 (DOI: 10.1021/acscentsci.1c00611)
- [30] Moses, I. A., Joshi, R., Ozdemir, B., Kumar, N., Eickholt, J., Barone, V. (2021). Machine Learning Screening of Metal-Ion Battery Electrode

- Materials. *ACS Appl. Mater. Interfaces*, 13(45), 53355–53362 (DOI: 10.1021/acsami.1c04627)
- [31] Zhang, H., Wang, Z., Cai, J., Wu, S., Li, J. (2021), Machine-learning-enabled tricks of the trade for rapid host material discovery in Li–S battery. *ACS Appl. Mater. Interfaces*, 13(45), 53388–53397 (DOI: 10.1021/acsami.1c10749)
- [32] Yan, H., Wei, M., Ma, J., Li, F., Evans, D. M., Duan, X. (2009), Theoretical study on the structural properties and relative stability of M(II)-Al layered double hydroxides based on a cluster model. *J. Phys. Chem. A*, 113(21), 6133–614 (DOI: 10.1021/jp810129h)
- [33] Berger, R. (2004). Computational Chemistry. Introduction to the theory and applications of molecular and quantum mechanics. Von Errol G. Lewars. *Angew. Chem.* (DOI: 10.1002/ange.200485057)
- [34] Hohenberg P., Kohn W. (1964), Inhomogeneous electron gas, *Phys. Rev. B*, 136, B864-B871 (DOI: 10.1103/PhysRev 136.B864)
- [35] Kohn W., Sham L. J. (1965), Self-consistent equations including exchange and correlation effects, *Phys. Rev.*, 140, A1133-A1138 (DOI: 10.1103/PhysRev 140.A1133)
- [36] Xia B. Y., Wu H.B., Wang X., Lou X.W. (2013), Index facets and enhanced electrocatalytic properties, *Angew. Chem. Int. Ed.*, 52, 12337-12340 (DOI: 10.1002/anie.201307518)
- [37] Kohn W., Sham L. J. (1965), Self-consistent equations including exchange and correlation effects, *Phys. Rev.*, 140, A1133-A1138 (DOI: 10.1103/PhysRev 140.A1133)
- [38] Zhao, G. L., Bagayoko, D., Williams, T. D. (1999), Local-density-approximation prediction of electronic properties of GaN, Si, C, and RuO₂, *Phys. Rev. B.*, 60, 1563–1572. (DOI:10.1103/physrevb.60.1563)
- [39] Martin, R.M. (2004) Electronic structure: basic theory and practical methods, Cambridge University press

- [40] Ceperley, D.M., Alder B. (1980), Ground State of the Electron Gas by a Stochastic Method, *J. Phys. Rev. Lett.*, 45, 566 (DOI: 10.1103/PhysRevLett.45.566)
- [41] Perdew, J. P., Chevary, J. A., Vosko, S. H., Koblak, J. A., Mark R, P., Singh, D. J., Fiolhais, Carlos. (1992), Atoms, molecules, solids, and surfaces: Applications of the generalized gradient approximation for exchange and correlation, *Phys. Rev. B.*, 46, 6671–6687 (DOI: 10.1103/physrevb.46.6671)
- [42] Becke, A. D. (1988), Density-functional exchange-energy approximation with correct asymptotic behaviour, *Phys. Rev. A.*, 38, 3098–3100. (DOI: 10.1103/PhysRevA.38.3098)
- [43] Lee, C., Yang, W., Parr, R. G. (1988), Development of the Colle-Salvetti correlation-energy formula into a functional of the electron density, *Phys. Rev. B.*, 37, 785–789. (DOI: 10.1103/PhysRevB.37.785)
- [44] Sholl, D. S., Steckel, J. A. (2023), Density functional theory, a practical introduction, 2nd Edition, *Wiley, New Jersey*, 50-55, (978-1-119-84086-2)
- [45] Larsen, A. H.; Mortensen, J. J.; Blomqvist, J.; Castelli, I. E.; Christensen, R.; Dulak, M.; Friis, J.; Groves, M. N.; Hammer, B.; Hargus, C.; Hermes, E. D.; Jennings, P. C.; Jensen, P. B.; Kermode, J.; Kitchin, J. R.; Kolsbjerg, E. L.; Kubal, J.; Kaasbjerg, K.; Lysgaard, S.; Maronsson, J. B.; Maxson, T.; Olsen, T.; Pastewka, L.; Peterson, A.; Rostgaard, C.; Schiøtz, J.; Schütt, O.; Strange, M.; Thygesen, K. S.; Vegge, T.; Vilhelmsen, L.; Walter, M.; Zeng, Z.; Jacobsen, K. W. The Atomic Simulation Environment-A python library for working with atoms. *J. Phys. Condens. Matter.* 2017, 29, 273002 (DOI: 10.1088/1361-648X/aa680e)
- [46] Hafner, J. (2008), *Ab-initio* simulations of materials using VASP: Density-functional theory and beyond. *J. Comput. Chem.*, 29(13), 2044–2078 (DOI: 10.1002/jcc.21057)

- [47] Kresse, G., Furthmüller, J. (1996), Efficient iterative schemes for *ab initio* total-energy calculations using a plane-wave basis set. *Phys. Rev.*, *54*(16), 11169–11186 (DOI: 10.1103/physrevb.54.11169)
- [48] Perdew, J. P., Burke, K., Ernzerhof, M. (1996), Generalized Gradient Approximation made simple. *Phys. Rev. Lett.*, *77*(18), 3865–3868 (DOI: 10.1103/physrevlett.77.3865)
- [49] Kresse, G., Joubert, D. P. (1999), From ultrasoft pseudopotentials to the projector augmented-wave method. *Phys. Rev. B*, *59*(3), 1758–1775 (DOI: 10.1103/physrevb.59.1758)
- [50] Blöchl, P. E. (1994), Projector augmented-wave method. *Phys. Rev. B*, *50*(24), 17953–17979 (DOI: 10.1103/physrevb.50.17953)
- [51] Grimme, S., Antony, J., Ehrlich, S., Krieg, H. (2010b), A consistent and accurate *ab initio* parametrization of density functional dispersion correction (DFT-D) for the 94 elements H-Pu. *J. Chem. Phys.*, *132*(15), 154104 (DOI: 10.1063/1.3382344)
- [52] Zhuo, Y., Tehrani, A. M., Brgoch, J. (2018), Predicting the Band Gaps of Inorganic Solids by Machine Learning. *J. Phys. Chem. Lett.*, *9*(7), 1668–1673 (DOI: 10.1021/acs.jpcclett.8b00124)
- [53] Wang, Z., Zhang, H., Li, J. (2021), Accelerated discovery of stable spinels in energy systems via machine learning. *Nano Energy*, *81*, 105665 (DOI: 10.1016/j.nanoen.2020.105665)
- [54] Xia, J., Zhao, L., Liao, M., Wu, Q. (2023), Rectangular transition metal-rTCNQ organic frameworks enabling polysulfide anchoring and fast electrocatalytic activity in Li-Sulfur batteries: A density functional theory perspective. *Molecules*, *28*(5), 2389 (DOI: 10.3390/molecules28052389)